文章编号：1001-9014(2022)03-0517-17

DOI：10. 11972/j. issn. 1001-9014. 2022. 03. 001

Recent progress on natural biomaterials boosting high-performance perovskite solar cells

XIONG Shao-Bing[1], BAO Qin-Ye[1*], CHU Jun-Hao[2]

(1. School of Physics and Electronic Science, East China Normal University, Shanghai 200241, China;
2. Department of Materials Science, Fudan University, Shanghai 200433, China)

Abstract: Perovskite solar cells (PeSCs) have been considered as one of the most promising photovoltaic technologies due to their high efficiency, low-cost and facile fabrication process. The power conversion efficiency and stability of PeSCs highly depend on the quality of perovskite film and the interfaces in the device, which are the main sources of PeSCs nonradiative recombination losses. Natural biomaterials, with the advantages of earth-abundance, non-toxicity, and biocompatibility, have shown huge potential to improve both perovskite layer and interfaces in PeSCs. Herein, the latest progress using natural biomaterials to achieve high-performance PeSCs is reviewed. It's discussed the roles of natural biomaterials on perovskite film in terms of morphology optimization, defect passivation and energetics modification. Meanwhile, the strategies using natural biomaterials to create a superior interface between the perovskite and charge transport layer, and to build stretchable, biocompatible, and biodegradable electrodes are present. Finally, an outlook on the further development of PeSCs with respect to natural biomaterials is provided.

Key words: perovskite solar cell, natural biomaterials, defect passivation, energetics modification

天然生物材料促进高性能钙钛矿太阳能电池的进展

熊少兵[1], 保秦烨[1*], 褚君浩[2]

(1. 华东师范大学物理与电子科学学院，上海 200241;
2. 复旦大学材料科学系，上海 200433)

摘要：钙钛矿太阳能电池(PeSCs)因其高效率、低成本和简单的制备工艺而被认为是最有前途的光伏技术之一。PeSCs的能量转换效率和稳定性很大程度上取决于钙钛矿薄膜的质量和器件中的界面，它们是PeSCs非辐射复合损失的主要来源。天然生物材料具有丰富的资源、无毒和生物相容性等优点，在改善PeSCs的钙钛矿层和界面方面显示出巨大的潜力。本文综述了利用天然生物材料实现高性能PeSCs的最新进展。首先讨论天然生物材料在钙钛矿薄膜的形貌优化、缺陷钝化和能级调控方面的作用；同时，讨论利用天然生物材料优化钙钛矿和电荷传输层之间的界面，以及构建可拉伸、可生物相容和可生物降解的电极的策略；最后，展望PeSCs在天然生物材料方面的进一步发展。

关 键 词：钙钛矿太阳能电池；天然生物材料；缺陷钝化；能级调控

中图分类号：O47　　**文献标识码**：A

Introduction

Metal halide perovskites (MHPs) have attracted tremendous attention of both academia and industry communities due to their outstanding optoelectronic merits of high light absorption coefficient[1-2], long electron-hole diffusion length[3-4], tunable bandgap[5-6], and small exciton binding energy[7]. Attributed to the excellent proper-

Received date: 2021-07-19, **revised date**: 2021-09-11　　**收稿日期**：2021-07-19，**修回日期**：2021-09-11

Foundation items: Supported by the National Science Foundation of China grant (21875067, 51811530011); the Fundamental Research Funds for the Central Universities, Shanghai Rising-Star (19QA1403100).

Biography: XIONG Shao-Bing (1995-), male, Hebi, Henan Province, Doctoral candidate, major in the device physics of perovskite solar cells. E-mail: 52171213003@stu. ecnu. edu. cn.

* **Corresponding author**: E-mail: qybao@clpm. ecnu. edu. cn

ties, the power conversion efficiency (PCE) of perovskite solar cells (PeSCs) has boosted to a certified value of 25.5% within a decade of efforts[8]. Combined with the advances in manufacturing such as low-cost raw materials[9-10], low-temperature and facile fabrication process[11-12], as well as scalable and flexible compatibility[13-15], PeSCs have become the vanguard of the new renewable and clean solar energy technologies.

In general, perovskite solar cells are composed of the sandwich structures, where the photogenerated carriers in the active layer must travel across the perovskite film, enter the charge transport layer, and finally are collected at the corresponding electrodes. The performances of the PeSCs are the results of the whole system, which requires each layer to collaborate well and all the interfaces to work fluently. However, due to the soft and ionic nature of the perovskite and rapid crystal growth process, numerous defects are inevitable to form at the surface and grain boundaries of perovskite film[16-17]. These defects can act as recombination centers, impeding carrier transport and thus confining the PCE of PeSCs[18-20]. The defects are sensitive to external stress including moisture, heat, light and bias, destroying the long-term stability of PeSCs[21-24]. Moreover, the interfaces in the device are other sources for nonradiative recombination due to unmatched interface energy level alignment, which set the ceiling of photovoltage and further limit the PCE of PeSCs[25-27].

Many strategies have been explored to break the limits by improving the perovskite film quality with fewer defects and modifying the interface energetics, such as additive engineering[28-29], post-treatment[30] and interface design[31-34]. Various functional materials including metal cations, polymers, ionic liquids and fullerene derivatives have been developed to assist the implement of these strategies[35-40]. Recently, natural biomaterials, which are abundant in raw materials, low-cost on fabrication, flexible and biocompatible even biodegradable for application, have been emerging in the field of green optoelectronics devices[41-44], especially for renewable energy technologies[45-49]. Biomaterials play versatile roles as additive to improve perovskite film, as interlayer to improve interface contact, as novel charge transport layer to facilitate carrier transport, even as electrode to improve flexibility (Fig. 1).

In this review, we retrospect recent progress of natural biomaterials used in PeSCs. In the first section, we introduce the roles of biomaterials on perovskite film including morphology optimization, defect passivation and energetics modification. The following section discusses the biomaterial-assisted perovskite interface. Finally, we give an outlook on the further development of PeSCs with respect to natural biomaterials.

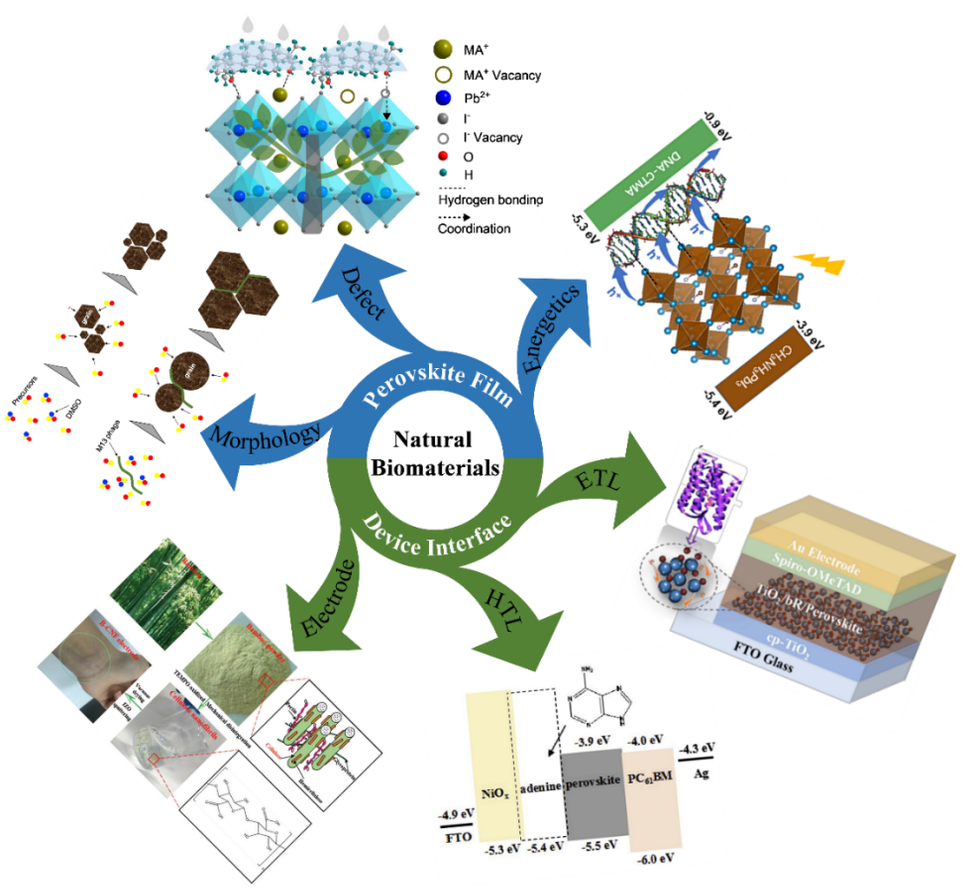

Fig. 1 Roles of natural biomaterials in PeSCs. ETL: electron transport layer; HTL: hole transport layer[50-55]
图1 天然生物材料在钙钛矿太阳能电池中的作用, ETL: 电子传输层;HTL: 空穴传输层[50-55]

1 Biomaterials-assisted perovskite film

1.1 Morphology optimization

Morphology, which refers to the uniformity, coverage, roughness, crystallinity and grain size of the film, is an important index to assess the quality of perovskite film. The perovskite film with poor morphology can greatly decrease the device performance by causing serious current leakage and substantial charge recombination losses[56-57]. The morphology of perovskite film can be well optimized by natural biomaterials in the way of additive engineering. Biomaterial additives can effectively modulate the perovskite crystallization kinetics, thereby prompting the formation of homogeneous and uniform perovskite film with larger grain size and fewer defect sites.

An interesting study of feeding "coffee" for perovskite film was performed by Wang and coworkers[58]. They introduced 1, 3, 7-trimethylxanthine, also named as caffeine, into the perovskite film to tune the morphology of perovskite film. It was found that the two conjugated carboxyl groups of caffeine as molecule locks could strongly interact with the unbonded Pb^{2+} ions, retarding perovskite crystal growth and forcing a preferred crystalline orientation (Fig. 2(a-b)). The morphology-improved perovskite presented reduced defect density and superior vertical charge transport efficiency, thus achieving a champion PCE of 20.25% in PeSCs, which was much higher than the control device with a PCE of 17.50% (Fig. 2(c)). Moreover, the non-volatile and thermal-stable caffeine significantly suppressed ion migration and increased the decomposition activation energy of perovskite. As a result, the caffeine containing PeSCs yielded excellent thermal stability (Fig. 2(d)), which remained over 85% of its initial efficiency after 1300 h heating at an elevated temperature of 85 ℃. However, the control device declined below 60% of its original PCE after only 175 h during the same condition.

Long-chain biopolymers with multiple functional groups can provide more interactions and stronger constraining force to modulate the morphological quality. Yang et al. added wood-based polymer, ethyl cellulose (EC), into the antisolvent to fabricate high quality perovskite film [49]. It was clearly displayed that EC biopolymer slowed down the crystallization process of perovskite film in Fig. 3(a), attributed to the Lewis acid-base interaction. The slower crystallization provided longer time for grains to grow and led to denser and smoother perovskite film with larger grain size (Fig. 3(b)). In addition, the long-chain EC provided a scaffold to eliminate the lattice strain of the annealing process and stabilized perovskite crystal structure (Fig. 3(c)). As a result, EC-modified devices achieved a high PCE of 19.41% compared to 17.11% for the control device. More importantly, EC-modified device showed enhanced environmental stability, which maintained 80% of its initial PCE after storage in ambient air at 45% relative humidity for 30 days, while the control device degraded completely for the same time. Lin and coworkers also employed M13 bacteriophage as perovskite nucleation and crystal growth template[50]. The carboxylic and amino groups on the surface of M13 bacteriophage gave numerous bonding sites to the uncoordinated Pb^{2+} in the perovskite, realizing a homogeneous perovskite film with enlarged grain size and favorable orientation (Fig. 3(d-e)). Consequently, the M13 bacteriophage templated perovskite solar cell delivered a PCE improvement from 17.8% to 20.1% with excellent reproducibility

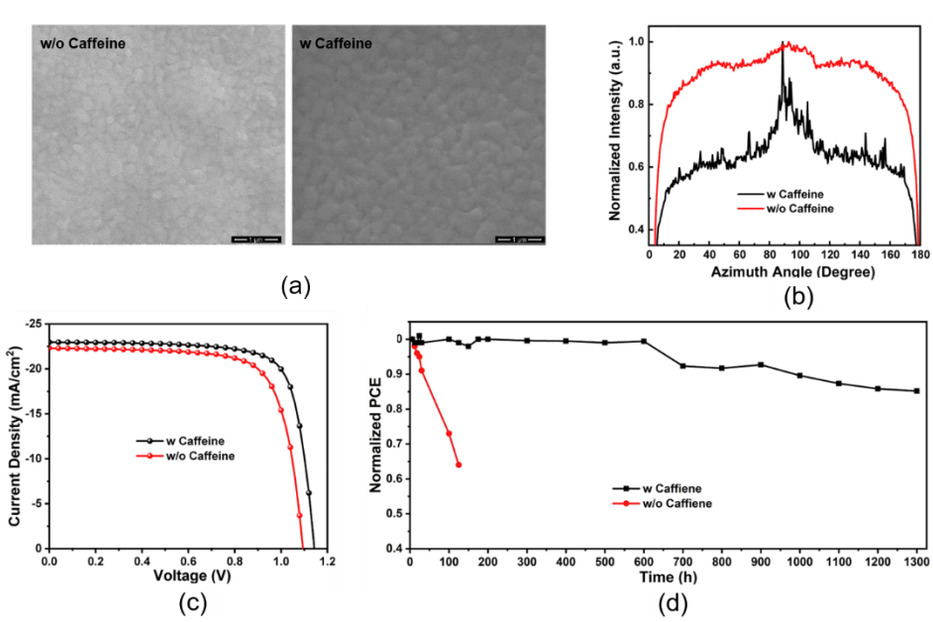

Fig. 2 (a) Morphology images of perovskite films with and without caffeine, (b) normalized azimuth angle plots along (110) crystal plane from the 2D grazing incidence wide-angle X-ray diffraction patterns of perovskite films with and without caffeine, (c) J-V curves of PeSCs with and without caffeine, (d) normalized PCE decays upon 85 ℃ continuous annealing in nitrogen box[58]

图2 (a)含咖啡因和不含咖啡因的钙钛矿薄膜的形貌图像,(b)含咖啡因和不含咖啡因的钙钛矿薄膜沿(110)晶面的二维掠入射广角x射线衍射图,(c)含咖啡因和不含咖啡因PeSCs的J-V曲线,(d)在氮气环境和85 ℃加热条件下PeSCs的归一化效率衰减曲线[58]

(Fig. 3(f)).

1.2 Defect passivation

Defects are usually formed when the growth of the crystal lattice is interrupted or misaligned, which are basically unavoidable in practical situation due to the soft and ionic nature of perovskite[16,59]. Diverse defects including vacancies, interstitials and anti-site substitutions exist at the surface and grain boundary of perovskite film, which can act as electronic trap states in the band gap of the perovskite and hence capture photogenerated carriers during PeSCs operation[17,60]. The defects also accelerate ion migrations, and reduce the splitting of quasi-Fermi levels, ultimately decreasing the device PCE[61-63]. Furthermore, defects are detrimental to the stability of perovskite films and solar cells[64-65]. Therefore, it is of great importance to minimize the defect density at the perovskite surface and grain boundary for the enhancement of both efficiency and stability of PeSCs.

Natural biomaterials show impressive capability to passivate defects in the perovskite. Xiong et al. employed forest-based biomaterial, betulin, as defect passivator for the first time and reached an PCE over 21% for p-i-n structured PeSCs (Fig. 4(a-b))[51]. In combination with experimental and theoretical analyses, they revealed that the hydroxyl group of betulin could effectively coordinate with the nonbonded Pb^{2+} ions by sharing a lone pair of electrons, which reduced the recombination sites and boosted charge transport. Moreover, the formation of hydrogen bonding between betulin and perovskite suppressed methylamine and halogen ions migration and stabilized the perovskite crystal structure, leading to largely enhanced operational stability. Qiu et al. also demonstrated biopolymer ploy-L-lysine (PLL) as effective defect passivator[66]. The large number of carboxylic and amino groups on the long chain of the biopolymer had a robust capability to chelate under-coordinated Pb^{2+} and suppress metallic Pb^0, resulting in a remarkable suppression of nonradiative recombination. As calculated by the density functional theory (DFT) in Fig. 4(c-h), the Pb-I antisite induced trap states were effectively annihilated with the adsorption of PLL, which neutralized the localized electron distribution by coordination effect. The substantial reduction of defects significantly improved the performance of blade-coated PeSCs, where the PLL passivated device showed a high efficiency of 19.45% and a high open-circuit voltage (V_{oc}) of 1.11 V, whereas the control device only had a PCE of 16.52% with a V_{oc} of 1.01 V.

Moreover, Hu et al. explored the relationship of passivation effect and molecule interaction strength by using a series of natural amino acid (NAA) molecules including glycine, glutamic acid, proline and arginine as precursor additive (Fig. 5(a))[67]. It was found that arginine with guanidine end group had the strongest coordination capability with the uncoordinated Pb^{2+} and thus showed the best passivation effect (Fig. 5(b-c)). Consequently, the arginine-passivated PeSCs exhibited a PCE of 20.49% with a V_{oc} increase over 100 meV. Recently, Wang and coworkers further demonstrated the impacts of molecule configuration on passivation effect by a set of biomaterials including theophylline, caffeine, and theobromine, which were accessible from the natural materials tea, coffee, and chocolate, respectively[48]. These nonvolatile biomolecules had the same functional groups of carbonyl group (C=O) and N - H, but the different chemical configurations. The detrimental effects of Pb-I

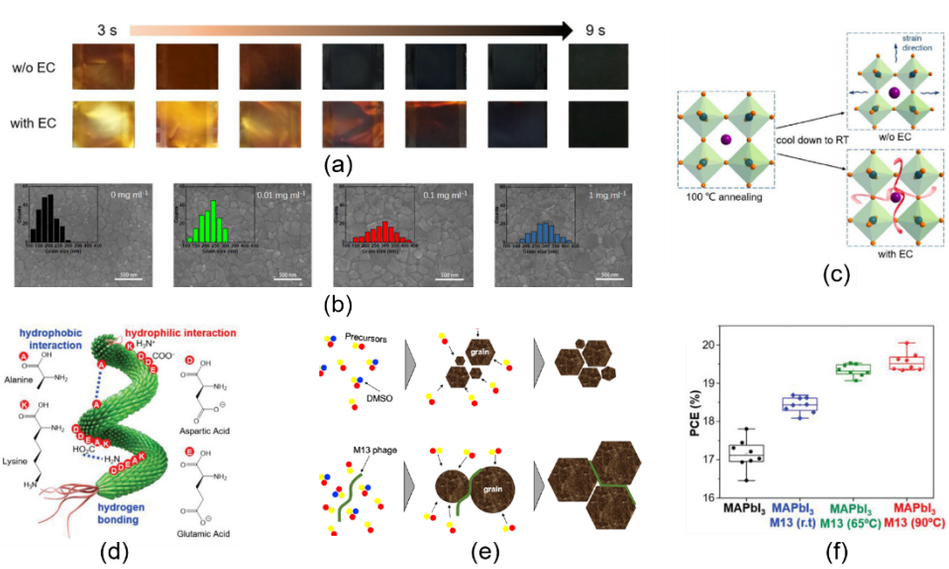

Fig. 3 (a) The crystallization process of perovskite films with and without EC under 100 °C annealing, (b) top-view SEM images of perovskite films with different EC concentrations, (c) the schematic diagram of the long-chain EC scaffold against expansion/shrinkage stress,[49] (d) chemical structure of M13 bacteriophage with multiple functional groups, (e) working mechanism of M13 bacteriophage-templated perovskite crystal growth, (f) PCE statistical analysis of PeSCs with M13 bacteriophage under different heat treatment[50]

图3 (a)在100 °C退火条件下,含EC和不含EC钙钛矿薄膜的结晶过程,(b)含不同EC浓度钙钛矿薄膜的SEM俯视图,(c)长链EC支架抗膨胀/收缩应力示意图[49],(d)多官能团M13噬菌体的化学结构,(e)基于M13噬菌体模板的钙钛矿晶体生长的工作机制,(f)含M13噬菌体的PeSCs在不同热处理条件下的PCE统计分析[50]

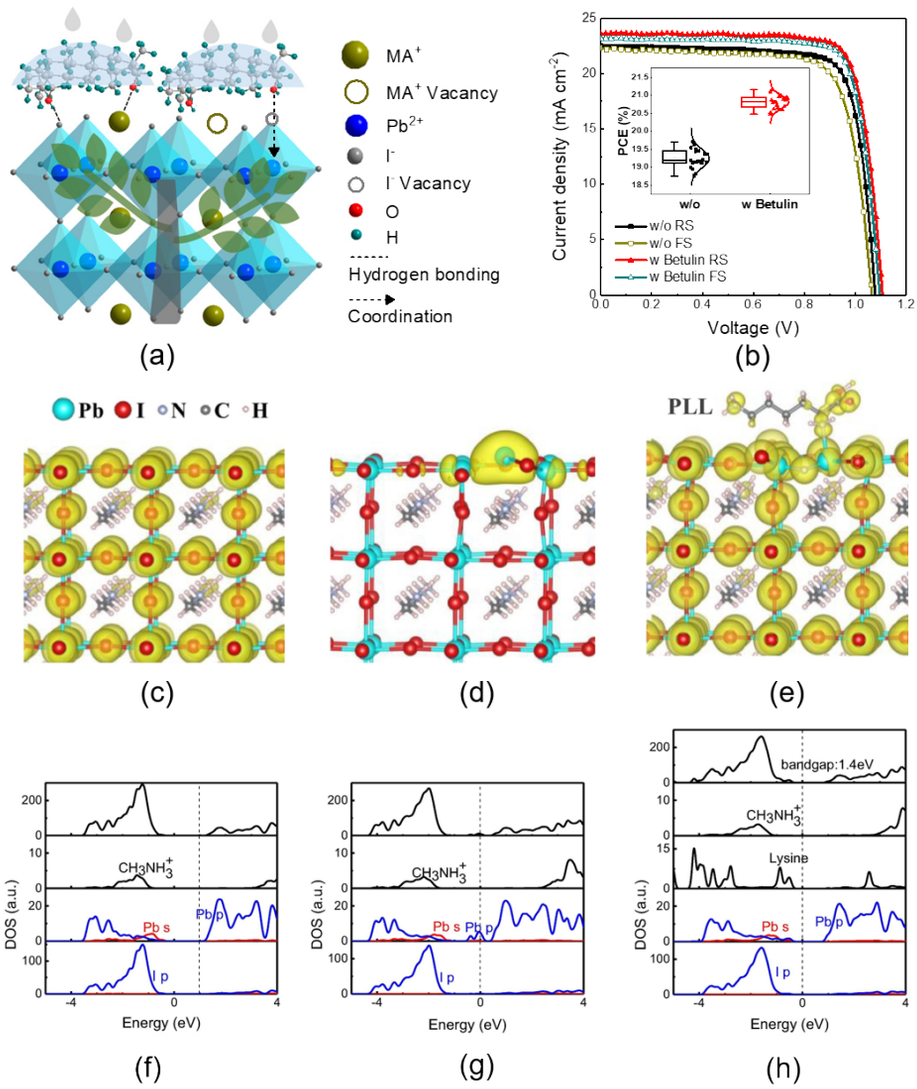

Fig. 4　(a) The schematic illumination of the interactions between forested-based biomaterial betulin and perovskite, (b) J-V curves of PeSCs with and without betulin under forward and reverse scan,[51] charge density distribution of $MAPbI_3$ (001) surface (c) with no defect, (d) with Pb-I antisite defect and (e) with Pb-I antisite defect after PLL passivating, density of states of $MAPbI_3$ (001) surface (f) with no defect, (g) with Pb-I antisite defect and (h) with Pb-I antisite defect after PLL passivating[66]

图 4　(a)森林基生物材料桦木素与钙钛矿相互作用示意图,(b)在正向和反向扫描下,含桦木素和不含桦木素的 PeSCs 的 J-V 曲线[51],在(c)没有缺陷、(d)有 Pb-I 反位缺陷以及(e)PLL 钝化 Pb-I 反位缺陷条件下的 $MAPbI_3$(001)晶面电荷密度分布,在(f)没有缺陷、(g)有 Pb-I 反位缺陷以及(h)PLL 钝化 Pb-I 反位缺陷条件下的 $MAPbI_3$(001)晶面态密度[66]

antisite were expected to be eliminated by the coordination interaction with C=O group, and the coordination strength was related to the hydrogen bonding between N-H and I of PbI_6^{2-} octahedron. The theophylline possessed the optimum configuration, where the hydrogen bonds enhanced the coordination interactions and led to the strongest interaction energy of -1.7 eV (Fig. 5(d)). For caffeine molecule, a methyl group replaced the H atom of N-H group, which broke the formation of hydrogen bonds with I ions, leading to a weaker interaction energy of -1.3 eV. Although the theobromine possessed both C=O and N-H groups, the distance between the two groups was too short, where the coordination impeded the formation of hydrogen bonds. The unfavorable configuration yielded an interaction energy as weak as -1.1 eV and might generate more defects due to the lattice distortion.

As a result, theophylline-passivated perovskite solar cells delivered the high efficiency of 23.48%, compared to 21.02% of the control device, 22.32% of caffeine-passivated device and 20.24% of theobromine-treated device (Fig. 5(e)), further confirming the crucial role of molecule configuration on passivation effectiveness and device performance. Meanwhile, the strong interactions between the theophylline and perovskite suppressed ions migration and thus enhanced operational stability. As shown in Fig. 5(f), theobromine-treated device maintained over 90% of its initial PCE under continuous light exposure for 500 h, while the control device declined over 80% during the same time.

1.3　Energetics modification

Electronic structures are the basic properties of a semiconductor, such as valence band (VB), conduction

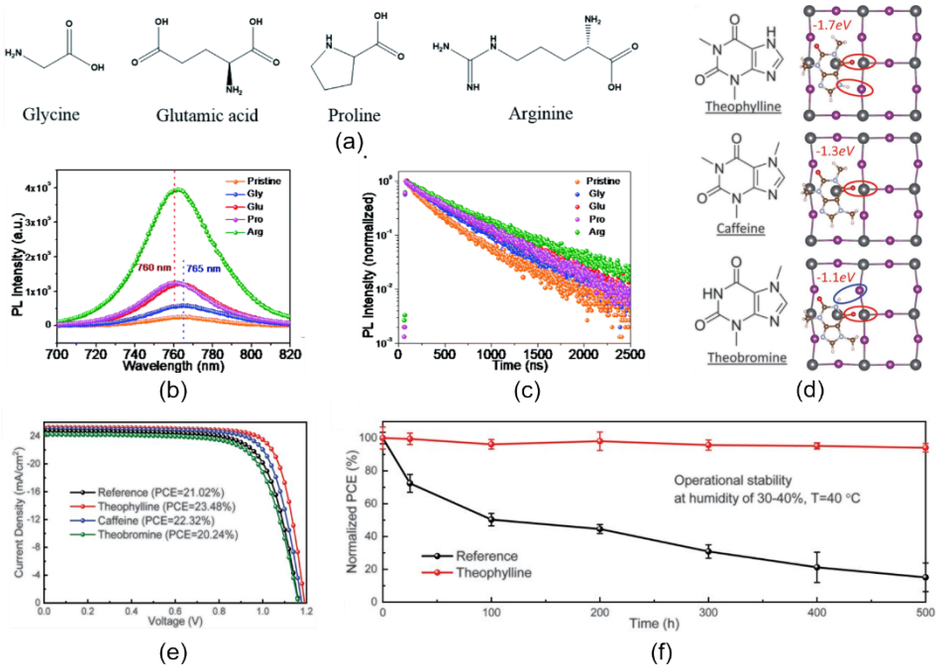

Fig. 5 (a) Chemical structure of natural amino acids (NAAs) molecules including glycine (Gly), glutamic acid (Glu), proline (Pro), and arginine (Arg), (b) steady-state and (c) time-resolved photoluminescence (PL) spectra of the pristine and various NAAs-passivated perovskite films,[67] (d) interaction structures of perovskite and theophylline, caffeine, and theobromine with corresponding theoretical interaction energy, (e) J-V curves of PeSCs with or without biomaterials' treatment under reverse scan direction, (f) normalized PCE decays of encapsulated PeSCs with or without theophylline treatment under continuous light (90 ± 10 mWcm^{-2}) exposure[48]

图5 (a)天然氨基酸(NAAs)分子的化学结构,包括甘氨酸(Gly)、谷氨酸(Glu)、脯氨酸(Pro)和精氨酸(Arg),原始和各种NAAs钝化的钙钛矿薄膜的(b)稳态和(c)时间分辨光致发光光谱[67],(d)钙钛矿与茶碱、咖啡因和可可碱的相互作用结构及其相应的理论相互作用能,(e)在反向扫描下,含生物材料和不含生物材料的PeSCs的J-V曲线,(f)在连续光照(90 ± 10 mWcm^{-2})下,经茶碱处理和不经茶碱处理的封装后PeSCs的归一化PCE衰变曲线[48]

band (CB), Fermi level (E_F) and vacuum level [68-69]. Perovskite with suitable electronic structures is essential to form favorable energy level alignment with adjacent charge transport layers and to improve charge transport in PeSCs [70-71]. A lot of work has demonstrated that the electronic structures of perovskite can be effectively tuned by self-doping effect, which prefer to be more n-type (or p-type) with rich PbI_2 (or MAI) in the film composition[72-73]. It was reported that the surface electronic structures of perovskites film heavily depended on the underlying work function (WF) of substrates (electrodes)[74-75]. Perovskite surface generally shows the higher WF when deposited on the higher WF substrate. The researchers also used molecule doping via natural biomaterials to adjust the energy level positions of perovskite and improve the performance of PeSCs.

Priya et al. introduced biomaterial deoxyribonucleic acid (DNA) into the perovskite precursor and obtained more p-type perovskite film with superior hole transport capability[52]. The Fermi level of the perovskite film is shifted from -4.91 to -5.01 eV after DNA incorporation. The highest occupied molecular orbital (HOMO) level of DNA matched with the VB of the perovskite, significantly prompting hole transport in the perovskite film. As confirmed by the steady-state photoluminescence (PL) spectra, a remarkable quenching was observed when the DNA-incorporated perovskite contacted with HTL. Therefore, the efficiency of DNA-based PeSCs (20.63%) was significantly improved compared to the control device (18.43%). Later, bioactive neurotransmitter dopamine was also introduced into the perovskite precursor to fabricate perovskite active layer with favorable energetics, reported by Zhang and coworkers[76]. They found a downshift of E_F toward VB for dopamine-incorporated perovskite film, accompanied by a valence band maximum (VBM) of -5.22 eV, which matched with the hole transport layer (-5.20 eV) compared with the pristine perovskite film with a VBM of -5.33 eV. The intimate contact facilitated hole transfer from the perovskite into HTL with a reduction of charge recombination, and largely increased the device performance.

Recently, Capsaicin, the compound that makes chili pepper spicy, was reported having a significant impact on the perovskite energetics by Xiong and coworkers. [77] They added a small amount of capsaicin into the perovskite precursor and systematically investigated the electronic structure of perovskite film. As shown in Fig. 6(a), the ultraviolet photoemission spectra (UPS) demonstrated a remarkable reduction of WF from 4.95 to 4.48 eV with the addition of 0.1 wt% capsaicin, while the energy difference between Fermi level and VBM increased by the same value, keeping a constant ionization potential. Such energy level shift indicated a clear energetics transformation from p-type to n-type for the perovskite top surface (Fig. 6(b)). Moreover, Kelvin probe force microscopy (KPFM) directly showed the for-

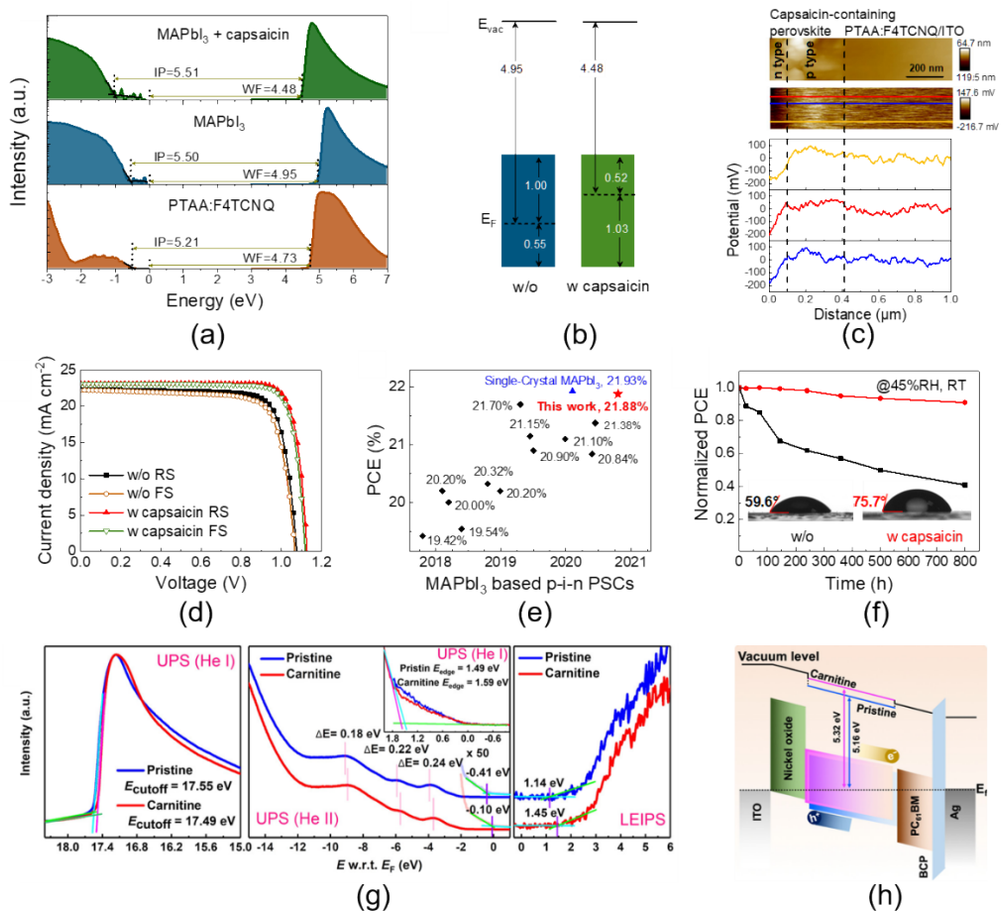

Fig. 6　(a) UPS spectra of secondary electron cutoff region and valence band region of PTAA:F4TCNQ, pristine perovskite and capsaicin-containing perovskite deposited on PTAA:F4TCNQ, (b) energy levels of perovskite with and without the capsaicin derived from UPS spectra, (c) cross-sectional AFM topographies, corresponding KPFM images, and potential profiles under zero-voltage bias of perovskite-capsaicin/PTAA:F4TCNQ/ITO, (d) J-V curves of PeSCs with or without the capsaicin under reverse and forward scan directions, (e) recent works on polycrystalline based and single-crystal $MAPbI_3$-based p-i-n PeSCs, (f) evolution of the PCEs measured from unencapsulated PeSCs in ambient air with 45% relative humidity (RH) at room temperature (RT),[77] (g) UPS spectra of secondary electron cutoff region (left panel), LEIPS spectra of valence band region (middle panel), and LEIPS spectra of conduction band region (right panel) of the perovskite films with and without the carnitine, (h) the schematic illustration of the energy levels of PeSCs with and without carnitine[78]

图 6　(a)PTAA:F4TCNQ、沉积在 PTAA:F4TCNQ 上的原始钙钛矿和含辣椒素钙钛矿的二次电子截止区和价带区的 UPS 能谱,(b)由 UPS 能谱得出的钙钛矿在添加和不添加辣椒素时的能级示意图,(c)钙钛矿-辣椒素/PTAA:F4TCNQ/ITO 的截面 AFM 形貌及在 0 V 偏压下对应的 KPFM 图像和电势变化曲线,(d)在正向和反向扫描下,掺杂辣椒素和不掺杂辣椒素 PeSCs 的 J-V 曲线,(e)近期基于多晶和单晶 $MAPbI_3$ 的 p-i-n 型 PeSCs 的研究[77],(f)在室温下和 45% 相对湿度的环境空气中,未封装的 PeSCs 的效率演变曲线,(g)含肉碱和不含肉碱钙钛矿薄膜的二次电子截止区 UPS 能谱(左)、价带区 LEIPS 能谱(中)和导带区 LEIPS 能谱(右),(h)含肉碱和不含肉碱的 PeSCs 的能级示意图[78]

mation of p-n junction below about 100 nm of the perovskite film surface (Fig. 6(c)). The resulting surface energetics formed a more efficient interface with the upper electron transport layer (n-type), boosting charge transfer in the device. Combined with the defect passivation effect of capsaicin, both defect-induced and interface nonradiative recombination were significantly suppressed. As a result, they achieved a record efficiency of 21.88% for $MAPbI_3$-based p-i-n perovskite solar cells with the high fill factor (FF) of 83.81% (Fig. 6(d-e)). Capsaicin also improved the device stability attributed to the enhanced water resistance ability of the perovskite film (Fig. 6(f)). In their another work, natural dyes were applied to tune the electronic structure of perovskite[79]. They introduced 5-chloroisatin (Isatin-Cl) as additive in the precursor and observed an n-type doping behavior for the perovskite film. The upshift of Fermi level produced more n-type perovskite, slowing down the rate of trap-mediated recombination and thus prolonging the carrier lifetime. Therefore, they obtained an enhanced efficiency of 20.18% with a negligible hysteresis and excellent stability.

Chen et al. also used natural vitamin B (carnitine) as an energetics modifier to fabricate high-performance PeSCs[78]. After the incorporation of vitamin B, it was observed that the WF increased by 150 meV, and the VBM shifted toward E_F by 100 meV, while the conduction band minimum (CBM) shifted away from the Fermi level

by 310 meV (Fig. 6(g)). Consequently, carnitine-incorporated perovskite film possessed a VBM of -5.42 eV and a CBM of -3.87 eV, closer with the HOMO (-5.40 eV) of hole transport layer and LUMO (-3.90 eV) of electron transport layer, respectively (Fig. 6(h)). The matched interfacial energy-level alignment caused high charge transfer efficiency at the interface, thereby suppressing interface charge recombination. Moreover, vitamin B could also annihilate both positive- and negative-charged ionic defects in the perovskite film. The combined effects led to grand enhancement of V_{oc} and FF, resulting in a PCE increased from 16.43% to 20.12%[78].

2 Biomaterials-assisted interface

Interface, which governs carrier extraction and collection in the devices, is of great importance to the efficiency and stability of PeSCs. An ideal interface generates no energy loss when carriers pass through the interface. Furthermore, interface should be robust enough with a strong barrier for ion migration, and oxygen and moisture permeation[80-82]. With this purpose in mind, the researchers put extensive efforts to improve interface contact, optimize interface energetics, and minimize interfacial trap states[83-86]. In this section, we focus on recent work of using biomaterials for interface engineering in PeSCs, in terms of electron transport layer, hole transport layer and stretchable electrode.

2.1 Electron transport layer

TiO_2 is common ETL in conventional n-i-p PeSCs due to its suitable electronic structures and brilliant chemical, electronical and optical properties[87-89]. However, tremendous oxygen vacancies on TiO_2 surface and the ultraviolet photocatalysis effect can trigger the decomposition of perovskite, leading to poor efficiency and stability of PeSCs[90]. You et al. utilized biopolymer heparin sodium (HS) as an interlayer anchored on TiO_2 surface (Fig. 7(a))[91]. They found that the HS biopolymer played multifunctional roles. First, HS biopolymer improved the morphology of TiO_2 film with no pinholes and better hydrophilicity, and also provided a favorable environment for perovskite film to growth, producing perovskite film with enlarged grain size and enhanced crystallinity (Fig. 7(b-c)). Moreover, the HS effectively passivated surface defects of TiO_2 film, and uncoordinated Pb^{2+} and I^- ions on the bottom surface of perovskite film. In addition, the strong anchoring effect of HS biopolymer could impede ions migration at TiO_2/$MAPbI_3$ interface, suppressing the hysteresis behavior (Fig. 7(d-

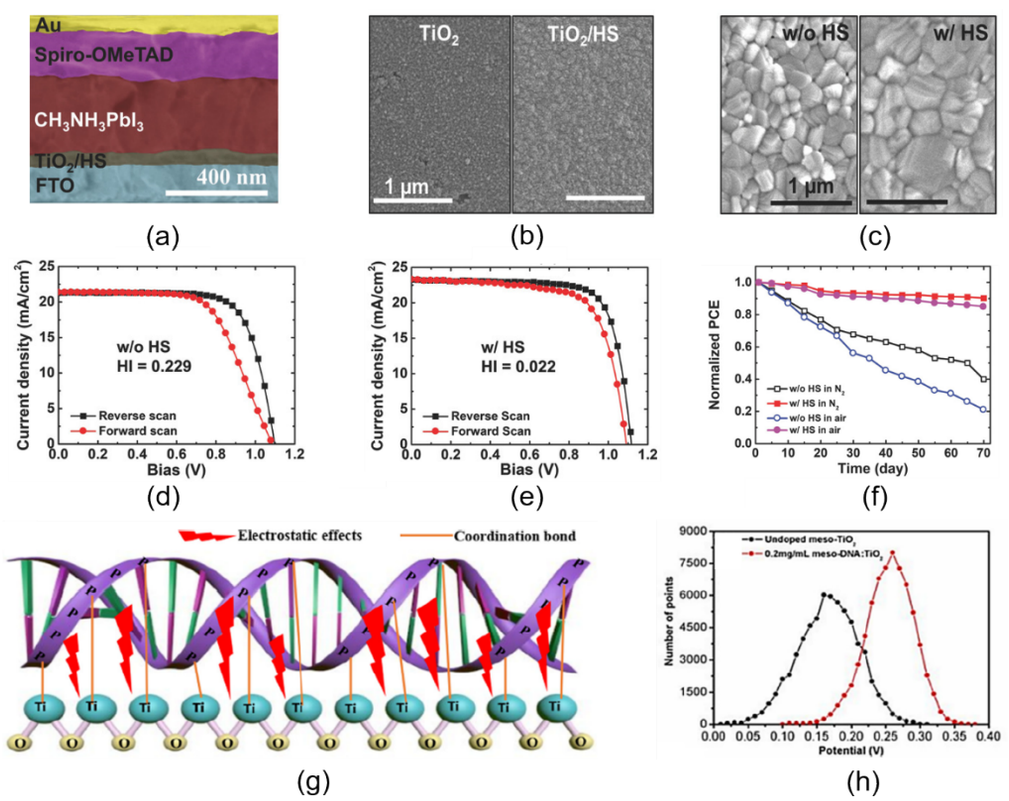

Fig. 7 (a) Cross-section SEM image of PeSCs with HS modified TiO_2, top-view SEM images of: (b) pristine and HS-modified TiO_2, and (c) perovskite films deposited on pristine and HS-modified TiO_2 substrates, J-V characteristics of PeSCs (d) without and (e) with HS layers under forward and reverse scan directions, (f) stability test of PeSCs without and with HS interlayers in N_2 and ambient environment,[91] (g) the schematic illumination of the interaction mechanism between DNA and meso-TiO_2, (h) the surface potential curves of undoped and DNA doped meso-TiO_2[92]

图7 基于HS修饰TiO_2的PeSCs的SEM截面图,(b)原始和HS修饰的TiO_2,以及(c)沉积在原始和HS修饰的TiO_2基底上的钙钛矿薄膜的SEM俯视图,(d)在正向和反向扫描下,无HS层和有HS层的PeSCs的J-V曲线,(f)在氮气和空气环境中,无HS层和有HS层的PeSCs的稳定性测试[91],(g)DNA与介孔二氧化钛相互作用机制的示意图,(h)未掺杂与DNA掺杂的介孔二氧化钛表面电势曲线[92]

e)). Therefore, they achieved an efficiency up to 20.1% for $MAPbI_3$ based solar cells with enhanced stability (Fig. 7(f)). Peng et al. demonstrated that deoxyribonucleic acid (DNA) could also reduce the trap states in TiO_2 by coordination bonding and electrostatic interactions (Fig. 7(g))[92]. Moreover, DNA enhanced the surface potential on TiO_2, improving carrier transport at the interface of the PeSCs (Fig. 7(h)).

Recently, Das et al. proposed a new type of bio-PeSCs[53], where natural biomaterials, bacteriorhodopsin (bR), are bridging perovskite and mesoporous TiO_2 ETL to enhance light energy conversion efficiency (Fig. 8(a-d)). The bR molecule incurred a Förster resonance energy transfer (FRET) process, and the photoexcited electrons could inject into the bR molecule layer and then quickly transfer to the TiO_2 cathode, serving as a carrier bridge between TiO_2 and perovskite layers. The bR molecule bridge significantly facilitated electron extraction in the PeSCs and restricted the interface charge recombination, leading to an enhancement of device performance.

Besides biopolymers, small biomaterials also exhibit excellent interfacial behaviors in PeSCs. Zhang et al. applied neurotransmitter (dopamine) to modify TiO_2, creating a cross-link between TiO_2 and perovskite (Fig. 9(a))[93]. Meanwhile, dopamine-modified TiO_2 had the closer CB to that of perovskite layer and the deeper VB due to the strong electron-donating ability of dopamine (Fig. 9(b)), which effectively enhanced photogenerated electrons in perovskite layer transfer into the TiO_2 ETL. On the other hand, the amino groups of dopamine could repair the uncoordinated Pb^{2+} and suppress Pb-I/Br antisite on perovskite surface, further reducing carrier recombination loss. Consequently, the energy level aligned interface with fewer trap states by dopamine remarkably boosted the efficiency to 20.93% compared to 18.15% of the control device. Moreover, the device with dopamine-capped TiO_2 as ETL retained 80% of the initial efficiency under continuous full-sun illumination in nitrogen atmosphere for 1200 h, showing excellent stability (Fig. 9(c)). In contrast, the control device displayed a severe degradation with the same test condition. Recently, Wang et al. reported that Chlorophyll was applied to modify TiO_2 ETL[94]. They introduced carboxy-chlorophyll derivative (C-Chl) into the mesoporous TiO_2 film and yielded a record PCE of 3.11% for lead-free $Cs_2AgBiBr_6$ double PeSCs. It was demonstrated that C-Chl enhanced electron transfer at ETL/perovskite interface and suppressed interface charge recombination. Bone-based biomaterial hydroxyapatite nanoparticles (HAP NPs) were also mixed with TiO_2 NPs to build a robust scaffold for perovskite deposition[95]. HAP NPs could absorb Pb ions due to the strong bonding between Pb^{2+} and PO_4^{3-}, hence effectively blocking the lead leakage into the environment (Fig. 9(d-e)), which was crucial for the future commercialization of PeSCs.

The ETL SnO_2 possesses high carrier mobility and can be deposited at low temperature[96-97]. However, the poor film crystallinity of SnO_2 creates numerous trap states, which triggers interface recombination and decreases the device performance[98]. Dopamine was proposed to modify the interfacial contact between SnO_2 and perovskite film by Hou and coworkers.[99] They prepared a self-assembled monolayer (SAM) of dopamine (DA) between SnO_2 and perovskite. Similar to the case of TiO_2, dopamine anchored on SnO_2 surface and passivated the defects on SnO_2 surface. Dopamine also improved the surface affinity of the SnO_2 film, providing a good template for perovskite growth and thus creating the high-

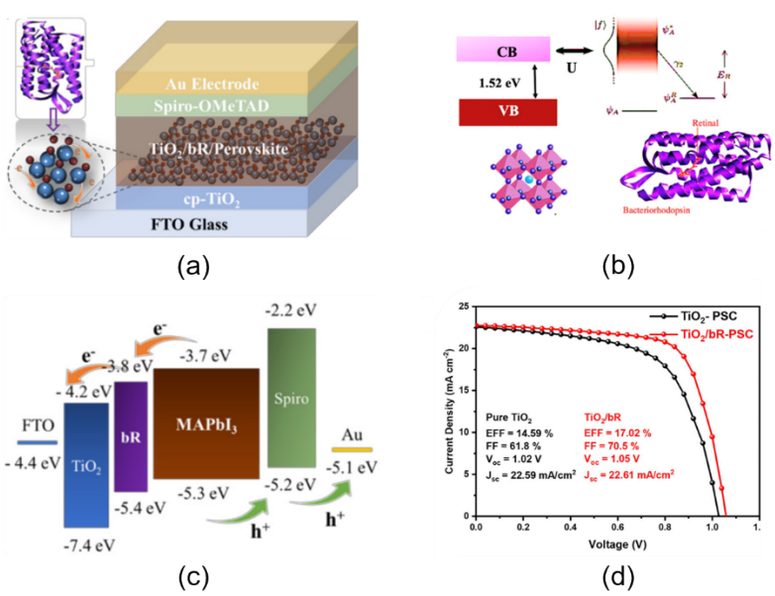

Fig. 8 (a) Device structure of the bio-PeSCs, (b) the schematics of the FRET process between perovskite and bR, (c) band alignment of the bio-PeSCs, (d) J–V curves of PeSCs with and without bR modification[53]

图8 (a)生物PeSCs的器件结构,(b)钙钛矿与bR之间的FRET原理图,(c)生物PeSCs的能级示意图,(d)bR修饰前后PeSCs的J–V曲线[53]

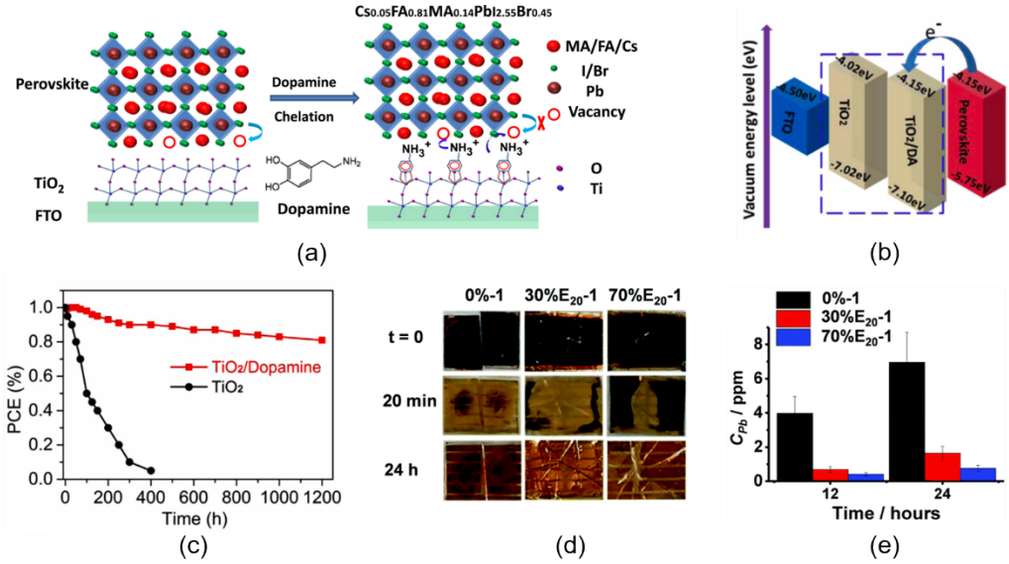

Fig. 9 (a) The schematic interactions of dopamine with perovskite and TiO_2 interface, (b) energy level diagram, (c) the normalized PCE change of PeSCs with TiO_2 and dopamine-capped TiO_2 as ETLs kept under continuous full-sun illumination in nitrogen atmosphere[93], (d) photographs and (e) Pb release concentrations of PeSCs with different HAP contents after the immersion in water for 0-24 h[95]

图9 (a)多巴胺与钙钛矿和TiO_2界面的相互作用示意图,(b)能级示意图,(c)在氮气气氛中和持续光照下,以TiO_2和多巴胺修饰的TiO_2为电子传输层的PeSCs的归一化PCE变化曲线[93],不同HAP含量的PeSCs在水中浸泡0~24 h后的(d)照片和(e)Pb释放浓度[95]

quality perovskite film with enlarged grain size and smoother surface. Dopamine could further reduce the WF of SnO_2 with the formation of an interfacial dipole, enhancing electron extraction at the interface. Kim et al. introduced a biomolecule SAM of creatine on the SnO_2 surface to improve ETL/perovskite interface (Fig. 10 (a))[100]. The creatine SAM layer also formed an interface dipole and reduced the WF of SnO_2 layer, resulting in an enhancement of carrier extraction (Fig. 10(b-c)). As a result, PeSCs with creatine interlayer yielded a high efficiency of 20. 8%.

Fullerene and its derivatives are the main organic materials used for ELT in inverted p-i-n PeSCs[101]. However, the large energy difference between the LUMO of PCBM and WF of metal electrodes impairs the electron collection efficiency at the cathode and limits the overall efficiency of PeSCs. Xiong et al. used natural biomaterials Isatin and its derivative Isatin-Cl (Fig. 10(d)) to optimize cathode interface[84]. The WF of Al electrode largely decreased when Isatin was inserted between PCBM and Al, attributed to the formation of a negative dipole at the interface (Fig. 10(e)). It significantly facilitated electron transfer and largely suppressed interface charge recombination at cathode back contact, leading to enhanced PeSCs efficiency (Fig. 10(f)).

2.2 Hole transport layer

Hole transport layer (HTL) takes the responsibility of hole transport and extraction during PeSCs operation. The HTLs generally include PEDOT: PSS, Spiro-OMeTAD, polytriarylamine (PTAA) and inorganic NiO_x[102]. Among them, Spiro-OMeTAD is considered to be the landmark during the development of PeSCs, which established all-solid PeSCs with a PCE over 10%[103]. However, Spiro-OMeTAD needs additional doping of bis (trifluoromethane) sulfonimidelithium salt (LiTFSI) and hydrophilic 4-tert-butylpyridine (tBP) to enhance solubility and hole mobility, which not only complicates the fabrication process but also brings poor stability due to the hygroscopic and diffusive nature of these dopants[102]. Therefore, there is urgent demand to develop cost-effective and dopant-free HTLs for highly efficient and stable PeSCs.

Li et al. demonstrated that natural photosynthetic catalyst Chlorophyll was feasible for hole transport in PeSCs[104]. They utilized zinc Chlorophyll aggregates, Chl-1 and Chl-2, as HTL without dopants, and then fabricated $CH_3NH_3PbI_{3-x}Cl_x$ based PeSCs with a PCE of 11. 44% (Fig. 11(a)). They found that zinc Chlorophyll aggregates could form type 1 alignment with perovskite layer, where the LUMO and HOMO levels of Chl-1 and Chl-2 aggregates were above that of perovskite, respectively (Fig. 11(b)), which was favorable for hole transfer (Fig. 11(c)). Later, Yusoff et al. employed DNA based biomaterial, DNA - hexadecyl trimethyl ammonium chloride (CTMA), as new type HTL in inverted PeSCs[105]. They achieved a high PCE of 15. 86% for the biomaterial-based inverted PeSCs compared to 12. 49% for PEDOT: PSS based devices. Moreover, DNA-CTMA film was low-temperature and solution processable, and exhibited high thermal stability, good wettability and excellent transparence over a wide range from 300 to 1100 nm, making it a good candidate HTL for high-performance PeSCs.

NiO_x is commonly used as HTL in inverted PeSCs with the advance of low cost and good stability, however, its high VBM level and poor conductivity largely restrict the device performance[106]. Recently, Xie et al. reported that natural biomaterial adenine was an excellent sur-

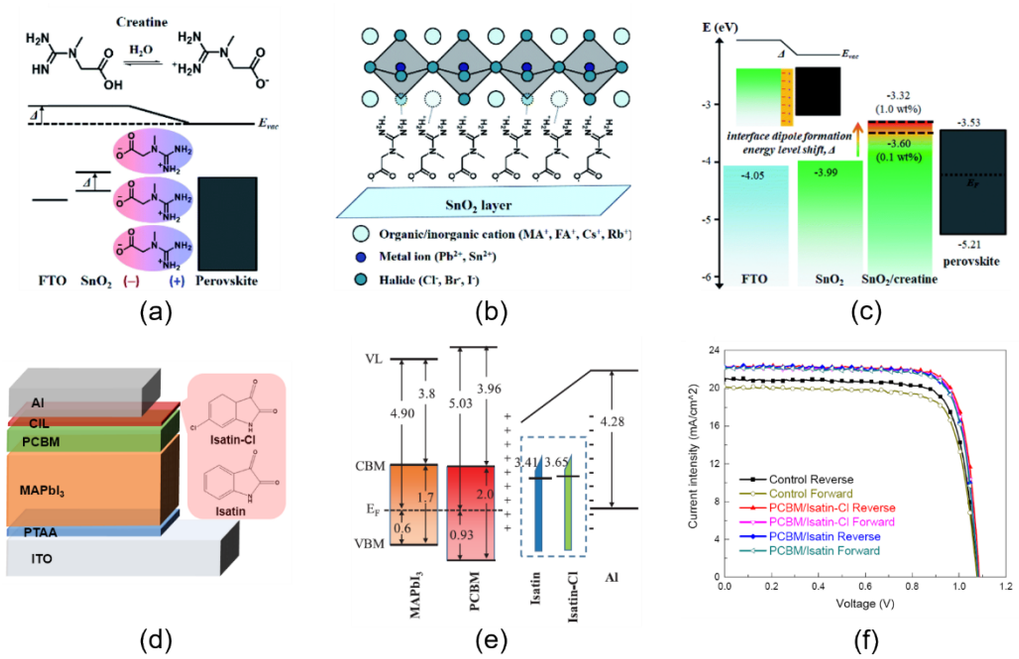

Fig. 10　(a) Dipole effect of creatine layer at the perovskite/SnO_2 interface, (b) defect passivation ability of the creatine layer, (c) energy level illustration of the UPS results,[100] (d) the schematic of device structure with Isatin and Isatin-Cl as cathode interlayer, (e) the energy level diagram, (f) J-V curves of pristine, Isatin and Isatin-Cl optimized devices under forward and reverse scan directions[84]

图 10　(a)肌酸层在钙钛矿/SnO_2界面的偶极子效应,(b)肌酸层的缺陷钝化作用,(c)UPS 能谱得出的能级示意图[100],(d)以 Isatin 和 Isatin-Cl 为阴极中间层的器件结构示意图,(e)能级示意图,(f)在正向和反向扫描下,原始、Isatin 和 Isatin-Cl 修饰后器件的 J-V 曲线[84]

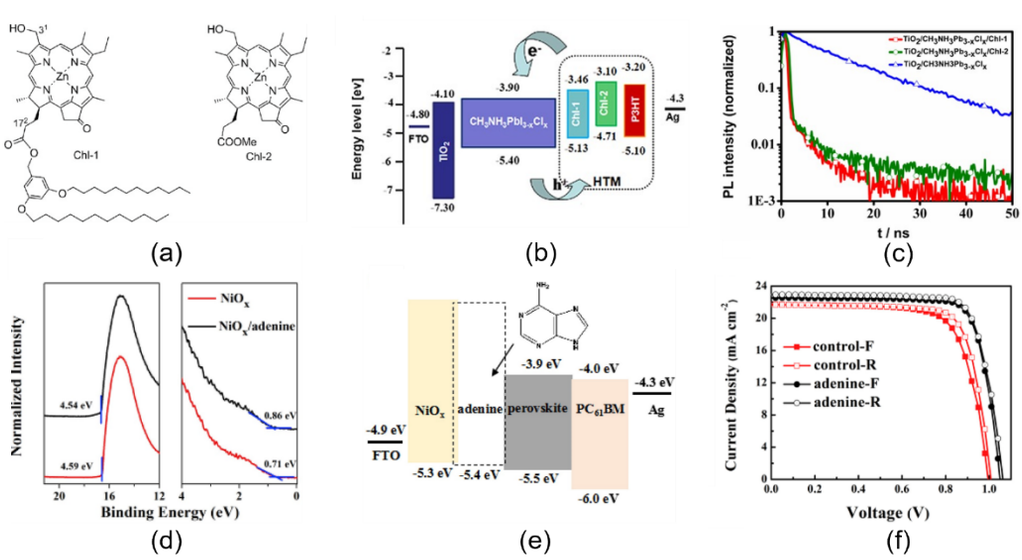

Fig. 11　(a) Molecular structures of zinc chlorophyll aggregates, Chl-1 and Chl-2, (b) the energy level diagram of PeSCs based on Chl-1, Chl-2, and P3HT as HTLs, (c) time-resolved PL decays,[104] (d) UPS spectra for NiO_x film before and after adenine modification, (e) the energy diagram of the device, (f) J-V curves of control and adenine-modified devices under forward and reverse scan directions[54]

图 11　(a)叶绿素锌聚集物 Chl-1 和 Chl-2 的分子结构,(b)以 Chl-1、Chl-2、P3HT 为空穴传输层的 PeSCs 能级图,(c)时间分辨 PL 衰变曲线[104],(d)腺嘌呤修饰前后 NiO_x膜的 UPS 能谱,(e)器件能级示意图,(f)在正向和反向扫描下,腺嘌呤修饰前后器件的 J-V 曲线[54]

face modifier for NiO_x HTL[54]. The adenine modification reduced the WF of NiO_x by 0.05 eV and increased the VBM of NiO_x from 0.71 to 0.86 eV, leading to a deeper VB level of 5.4 eV than the pristine NiO_x film (5.3 eV) (Fig. 11(d-e)). The resulting energetics enhanced the hole extraction efficiency of NiO_x HTL. Moreover, the perovskite film deposited on the adenine modified NiO_x film showed larger grain size and better crystallinity, attributed to the improved wettability of NiO_x surface. Therefore, a significant increase of PCE from 16.76% to

18.96% with suppressed hysteresis behavior was obtained (Fig. 11(f)).

PEDOT:PSS is also widely used in the inverted PeSCs due to its facile and soluble fabrication process. However, its low WF limits the device photovoltage, and the acidic nature of PEDOT:PSS is also detrimental to the long-term stability of PeSCs[107-108]. To overcome the drawbacks of PEDOT:PSS, Li and workers introduced dopamine (DA) into PEDOT:PSS aqueous solutions[109]. The WF of PEDOT:PSS was surprisingly increased from 5.1 to 5.33 eV after doping dopamine, and the PH value raised from 1.5 to 5.2. The improved WF matched well with the VB of perovskite (5.4 eV), facilitating charge transfer and eliminating the photovoltage limit (Fig. 12(a)). Consequently, the dopamine-modified solar cell achieved a much higher V_{oc} of 1.08 V and PCE of 16.6%, while the control devices only had a V_{oc} of 0.96 V and PCE of 15.2%. The mild PH value of dopamine-modified PEDOT:PSS delivered less acid corrosion and impeded the degradation of perovskite, endowing the optimized device longer lifetime. Recently, they further investigated the working mechanism of dopamine doping PEDOT:PSS [110]. Electron spin resonance (ESR) measurement revealed that more radical content formed in dopamine doped PEDOT:PSS, which provided stronger electron donating capability (Fig. 12(b-c)). The amino and hydroxyl groups of dopamine were found to interact with the undercoordinated Pb^{2+} on perovskite bottom surface and improved the quality of the perovskite films, minimizing trap sites and suppressing trap-assisted recombination. Eventually, a champion efficiency up to 18.5% was realized for dopamine-modified PEDOT:PSS based PeSCs with enhanced stability (Fig. 12(d-e)).

2.3 Stretchable electrode

Stretchable electrodes play a key role in flexible PeSCs and the further application of PeSCs in wearable electronic devices. The commonly used flexible electrodes are based on silver nanowire networks or copper conductors, which are usually coated on plastic substrates such as polyethylene terephthalate (PET) and polyethylene naphthalate (PEN)[111-112]. Although these electrodes exhibit good stretchable capability and mechanical stability, the plastic substrates are hard to degrade in the environment and will cause white pollutions. Therefore, biomaterial-based flexible electrodes attract more attention due to their environmental harmless, biodegradable and biocompatible ability.

Cellulose paper, as a mature technique, is low-cost, light-weight, flexible, biocompatible and totally biodegradable, making it being an attractive substrate for flexible devices, which has been used in flexible sensors and organic solar cells. In 2018, Gao et al. employed carbon-modified cellulose paper as anode electrode and fabricated HTL-free flexible PeSCs for the first time

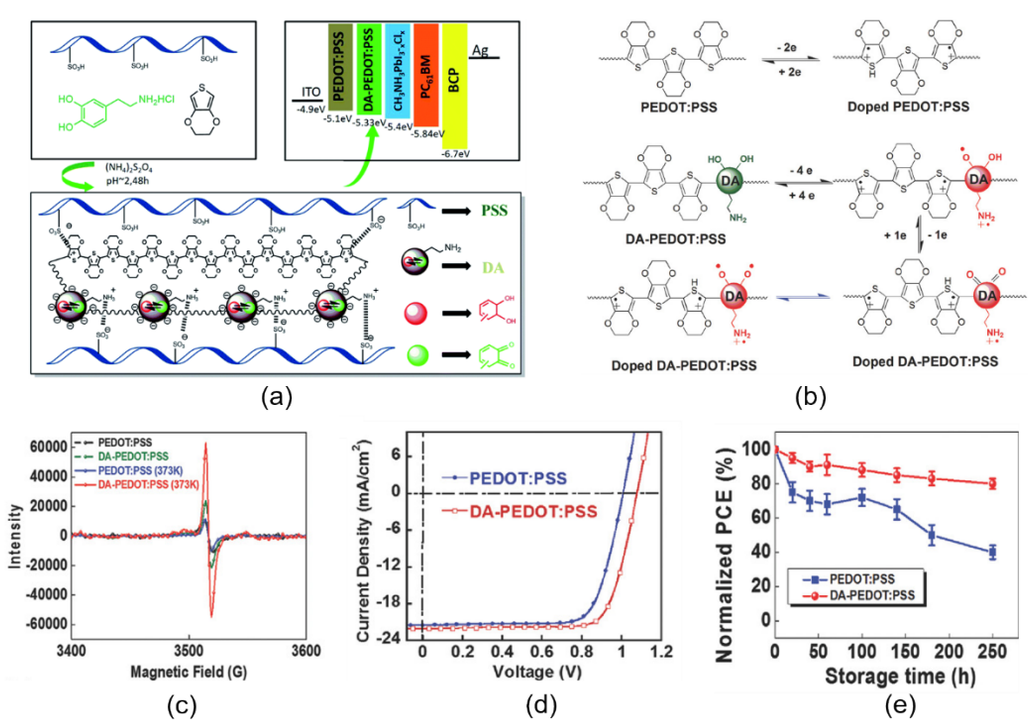

Fig. 12 (a) Synthesis condition, copolymer of DA-PEDOT:PSS, and energy levels of PEDOT:PSS and DA-PEDOT:PSS in PeSCs,[109] (b) considerable differences in doping of PEDOT:PSS and DA-PEDOT:PSS, (c) ESR spectra of PEDOT:PSS and DA-PEDOT:PSS at room temperature and 373 K, respectively, (d) J-V curves of PEDOT:PSS and DA-modified PEDOT:PSS based PeSCs, (e) long-term stability of PeSCs with PEDOT:PSS and DA-modified PEDOT:PSS HTLs in air under ambient conditions (temperature ≈ 25 ℃, humidity ≈ 40%)[110]

图12 (a)共聚物DA-PEDOT:PSS的合成条件以及PEDOT:PSS和DA-PEDOT:PSS在PeSCs中的能级[109],(b)PEDOT:PSS和DA-PEDOT:PSS的掺杂差异,(c)PEDOT:PSS和DA-PEDOT:PSS分别在室温和373 K下的ESR谱,(d)基于PEDOT:PSS和DA-PEDOT:PSS的PeSCs的J-V曲线,(e)基于PEDOT:PSS和DA-PEDOT:PSS的PeSCs在空气环境中(温度≈25 ℃,湿度≈40%)的长期稳定性[110]

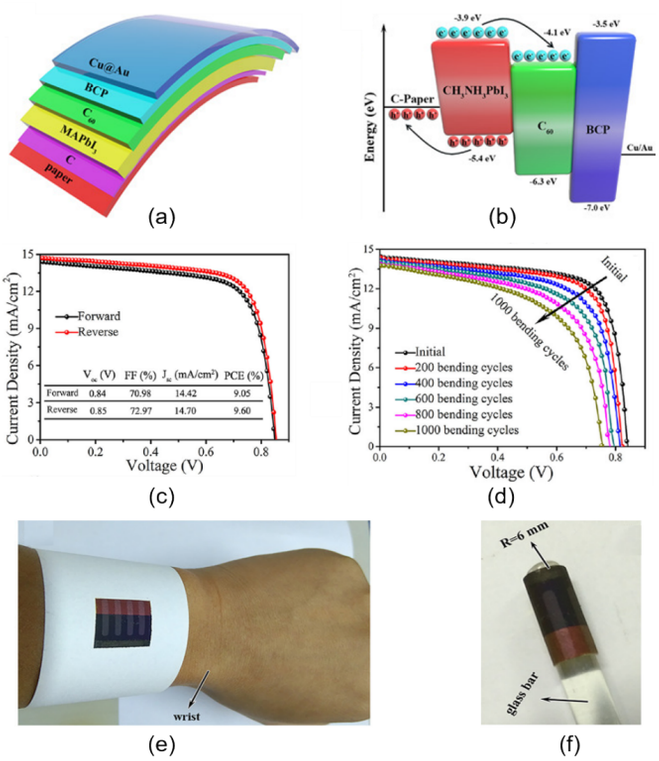

Fig. 13　(a) Device structure of paper based HTM-free PeSCs and (b) corresponding energy level diagram, (c) photovoltaic performance of paper based HTM-free PeSCs under forward and reverse scan directions, (d) J-V curves of paper based device with different bending cycles, (e) optical image of paper based HTM-free PeSCs attached on the wrist and (f) bent with radius (R) of 6 mm[113]

图 13　(a)纸基无空穴传输层的 PeSCs 的器件结构图及(b)相应的能级图,(c)在正向和反向扫描下,纸基无空穴传输层的 PeSCs 的光伏性能,(d)不同弯曲周期的纸基器件的 J-V 曲线,(e)粘贴在手腕上的无空穴传输层的纸基 PeSCs 的光学图像,(f)弯曲半径 R 为 6 mm[113]

(Fig. 13(a))[113]. The carbon-modified paper showed not only good conductivity but also proper energy level alignment with perovskite layer with the resulting efficient charge extraction (Fig. 13(b)). Based on the bio-substrate, they achieved a PCE of 9.05% for the HTL-free flexible PeSCs, with excellent flexibility and robust mechanical durability (Fig. 13(c-f)). However, the poor transmittance of carbon modified cellulose paper limits its application. Later, Zou and coworkers reported a transparent and stretchable electrode derived from bamboo and then fabricated flexible PeSCs with a PCE up to 11.68%[55]. Bamboo has tremendous highly-polymerized cellulose fibers, producing cellulose nanofibril substrates (B-CNF) (Fig. 14(a)). The B-CNF substrate showed superior transmittance over the full visible light range due to the presence of numerous carboxylate groups in B-CNT. Combined with the transparent conductive indium zinc oxide (IZO), the B-CNT/IZO electrode successfully integrated the merits of good transmittance, high conductivity and ultra-flexibility as well as extremely light weight. Moreover, the compact and smooth B-CNT/IZO electrode presented excellent mechanical stability, which could remain a stable and reliable square resistance after 3000 times bending with a 4 mm curvature radius, while the square resistance of PET/IZO electrode largely increased after 2400 times same bending (Fig. 14(b-c)). Furthermore, the B-CNT/IZO bioelectrode based PeSCs also delivered remarkable bendable fatigue resistance during the bending process (Fig. 14(d)). Han et al. recently demonstrated the practical feasibility of virus-templated gold nanowire electrodes for flexible PeSCs (Fig. 15(a))[114]. They used wild-type M13 bacteriophages as substrate for gold nanowire, which could bind to gold ions via ion exchange. The bioelectrode showed considerable conductivity and transparency, leading to a PCE of 9.28% with negligible hysteresis and brilliant stretchable ability (Fig. 15(b-d)).

3　Summary and outlook

In this review, we have summarized recent progress of natural biomaterials boosting highly efficient and stable PeSCs. Natural biomaterials play significant roles in active layer and interface of PeSCs. For the active layer, various natural biomaterials have been successfully introduced into the perovskite precursor to improve morphology, reduce trap density, and modify electronic structure of perovskite films, increasing device efficiency. The mechanism behind the improved perovskite film quality includes multiple factors such as retarded crystallization process, defect passivation via various functional groups and doping behavior. Natural materials also benefit for the long-term stability of PeSCs, attributed to the elimination of vulnerable defects and the enhancement of perovskite crystal structure. In terms of interface, natural biomaterials are effectively applied as buffer layer and charge transport layer to improve interface contact and hence minimize interface charge recombination loss in PeSCs. The mechanism behind the enhanced interface properties is mainly ascribed to the favorable energy level alignment induced by natural biomaterials, boosting charge transfer at the interface. Furthermore, natural biomaterials-based electrodes show excellent flexibility, strong stretchable ability, brilliant biocompatibility and biodegradability, which are suable for the fabrication of flexible and wearable PeSCs.

In fact, the performance of biomaterials-based PeSCs still lags behind the chemicals-based counterparts. To further improve the efficiency and stability of biomaterials-based PeSCs, in-depth understand of interactions between biomaterials and perovskite should be carefully investigated. The mechanism behind biomaterials-assisted perovskite formation and interface optimization is still unclear. Further exploration of novel biomaterials is highly required for the customized demands of PeSCs. Meanwhile, we also hope the application of natural biomaterials in lead-free PeSCs. The integration of green and biodegradable biomaterials with the nontoxic perovskite would fabricate the full green PeSCs with high efficiency and long-term stability.

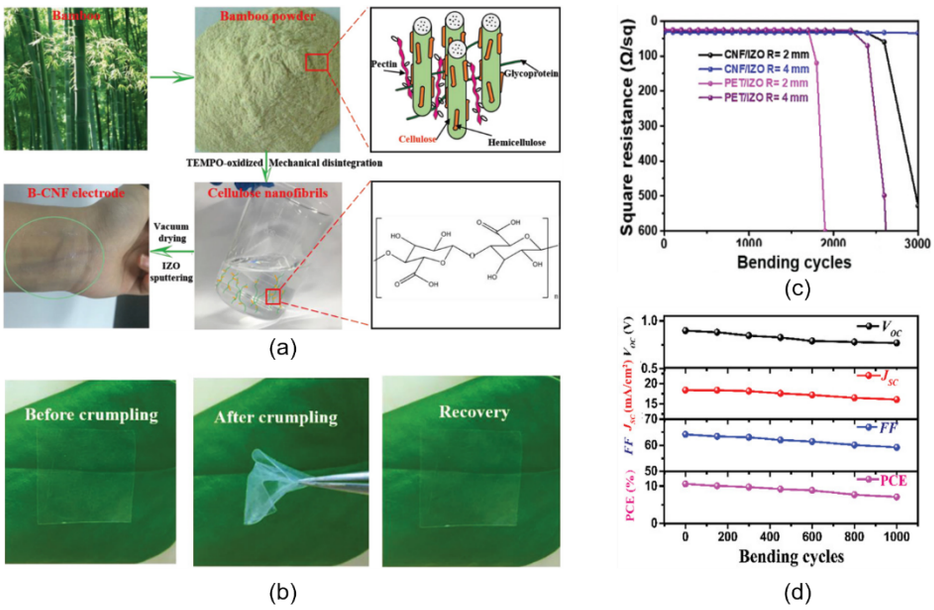

Fig. 14 (a) Preparation process of bamboo-derived cellulose nanofibril (b-CNF) electrodes, (b) photographs of b-CNF/IZO electrode recovery from random crumpling, (c) square resistance of b-CNF/IZO and PET/IZO electrode bending at different curvature radii, (d) the main parameters' variation of the flexible PeSCs upon periodic bending tests of a 4 mm curvature radius[55]

图 14 (a)竹源纤维素纳米纤维(b-CNF)电极的制备工艺,(b)b-CNF/IZO 电极从随机皱折中恢复的照片,(c)b-CNF/IZO 和 PET/IZO 电极在不同曲率半径下弯曲时的方阻,(d)在曲率半径为 4 mm 的情况下,周期性弯曲试验中柔性 PeSCs 的主要参数变化[55]

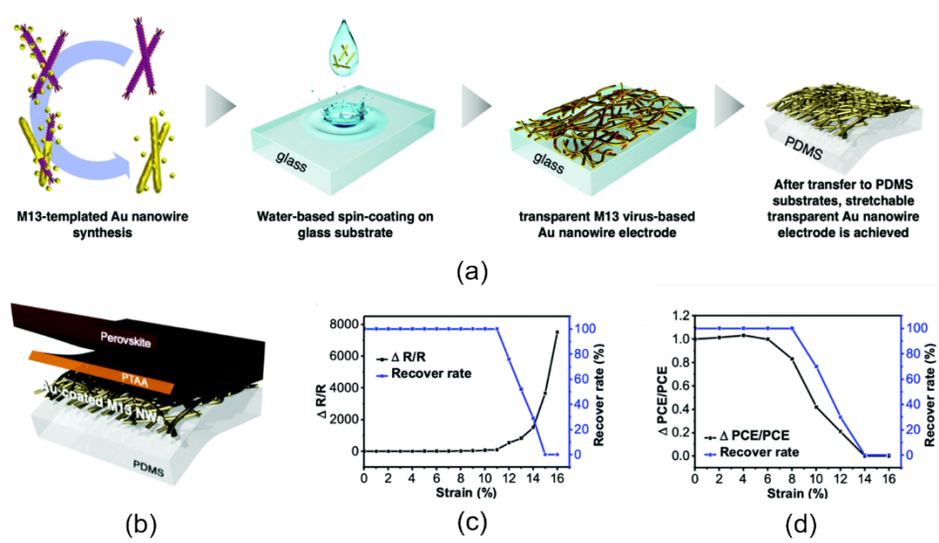

Fig 15 (a) The schematic illustration of preparation process of M13 bacteriophage-templated gold nanowire electrode, (b) illustrations of the virus-templated Au nanowires on PDMS with PTAA and perovskite layers, (c) stretchable ability test of M13 virus-templated Au nanowire electrode, (d) stretchable ability test of M13 virus-templated Au nanowire-based PeSCs[114]

图 15 (a)基于 M13 噬菌体模板的金纳米线电极制备工艺示意图,(b)在 PDMS 上的基于病毒模板的金纳米线的示意图,(c)基于 M13 病毒模板的金纳米线电极拉伸能力测试,(d)基于 M13 病毒模板的金纳米线电极的 PeSCs 拉伸能力测试[114]

References

[1] Yin W J, Shi T, Yan Y. Unique properties of halide perovskites as possible origins of the superior solar cell performance [J]. *Adv. Mater.* 2014, **26**(27): 4653-4658.

[2] Lee J W, Seol D J, Cho A N, *et al*. High-efficiency perovskite solar cells based on the black polymorph of $HC(NH_2)_2PbI_3$ [J]. *Adv. Mater.* 2014, **26**(29): 4991-4998.

[3] Stranks S D, Eperon G E, Grancini G, *et al*. Electron-hole diffusion lengths exceeding 1 micrometer in an organometal trihalide perovskite absorber [J]. *Science* 2013, **342**(6156): 341-344.

[4] Xing G, Mathews N, Sun S, *et al*. Long-range balanced electron- and hole-transport lengths in organic-inorganic $CH_3NH_3PbI_3$ [J]. *Science* 2013, **342**(6156): 344-347.

[5] Eperon G E, Stranks S D, Menelaou C, *et al*. Formamidinium lead trihalide: a broadly tunable perovskite for efficient planar heterojunction solar cells [J]. *Energy Environ. Sci.* 2014, **7**(3): 982-988.

[6] Saliba M, Correa Baena J P, Grätzel M, *et al*. Perovskite solar cells: from the atomic level to film quality and device performance [J]. *Angew. Chem.*, Int. Ed. 2018, **57**(10): 2554-2569.

[7] Yang Z, Surrente A, Galkowski K, *et al*. Unraveling the exciton binding energy and the dielectric constant in single-crystal methylammonium lead triiodide perovskite [J]. J. *Phys. Chem. Lett.* 2017, **8**(8): 1851-1855.

[8] NREL, Best Research-Cell Efficiencies, www. nrel. gov/pv/assets/

pdfs/best-research-cell-efficiencies. 20200925. pdf, accessed: Sep. 2020.
[9] Hou Y, Du X, Scheiner S, *et al*. A generic interface to reduce the efficiency-stability-cost gap of perovskite solar cells [J]. *Science* 2017, **358**(6367): 1192-1197.
[10] Song Z, McElvany C L, Phillips A B, *et al*. A technoeconomic analysis of perovskite solar module manufacturing with low-cost materials and techniques [J]. *Energy Environ. Sci*. 2017, **10**(6): 1297-1305.
[11] You J, Hong Z, Yang Y, *et al*. Low-temperature solution-processed perovskite solar cells with high efficiency and flexibility [J]. *ACS Nano* 2014, **8**(2): 1674-1680.
[12] Wang P, Wu Y, Cai B, *et al*. Solution-processable perovskite solar cells toward commercialization: progress and challenges [J]. *Adv. Funct. Mater*. 2019, **29**(47): 1807661.
[13] Li Z, Klein T R, Kim D H, *et al*. Scalable fabrication of perovskite solar cells [J]. *Nat. Rev. Mater*. 2018, **3**(4): 18017.
[14] Dou B, Whitaker J B, Bruening K, *et al*. Roll-to-roll printing of perovskite solar cells [J]. *ACS Energy Lett*. 2018, **3**(10): 2558-2565.
[15] Feng J, Zhu X, Yang Z, *et al*. Record efficiency stable flexible perovskite solar cell using effective additive assistant strategy [J]. *Adv. Mater*. 2018, **30**(35): 1801418.
[16] Ball J M, Petrozza A. Defects in perovskite-halides and their effects in solar cells [J]. *Nat. Energy* 2016, **1**(11): 16149.
[17] Jin H, Debroye E, Keshavarz M, *et al*. It's a trap! On the nature of localised states and charge trapping in lead halide perovskites [J]. *Mater. Horiz*. 2020, **7**(2): 397-410.
[18] Wetzelaer G J A, Scheepers M, Sempere A M, *et al*. Trap-assisted non-radiative recombination in organic-inorganic perovskite solar cells [J]. *Adv. Mater*. 2015, **27**(11): 1837-1841.
[19] Ran C, Xu J, Gao W, *et al*. Defects in metal triiodide perovskite materials towards high-performance solar cells: origin, impact, characterization, and engineering [J]. *Chem. Soc. Rev*. 2018, **47**(12): 4581-4610.
[20] Landi G, Neitzert H C, Barone C, *et al*. Correlation between electronic defect states distribution and device performance of perovskite solar cells [J]. *Adv. Sci*. 2017, **4**(10): 1700183.
[21] Lin Y, Liu Y, Chen S, *et al*. Revealing defective nanostructured surfaces and their impact on the intrinsic stability of hybrid perovskites [J]. *Energy Environ. Sci*. 2021, **14**(3): 1563-1572.
[22] Yang J, Hong Q, Yuan Z, *et al*. Unraveling photostability of mixed cation perovskite films in extreme environment [J]. *Adv. Opt. Mater*. 2018, **6**(20): 1800262.
[23] Yang J, Yuan Z, Liu X, *et al*. Oxygen-and water-induced energetics degradation in organometal halide perovskites [J]. *ACS Appl. Mater. Interfaces* 2018, **10**(18): 16225-16230.
[24] Yang J, Liu X, Zhang Y, *et al*. Comprehensive understanding of heat-induced degradation of triple-cation mixed halide perovskite for a robust solar cell [J]. *Nano Energy 2018*, 54: 218-226.
[25] Stolterfoht M, Caprioglio P, Wolff C M, *et al*. The impact of energy alignment and interfacial recombination on the internal and external open-circuit voltage of perovskite solar cells [J]. *Energy Environ. Sci*. 2019, **12**(9): 2778-2788.
[26] Gelmetti I, Montcada N F, Pérez-Rodríguez A, *et al*. Energy alignment and recombination in perovskite solar cells: weighted influence on the open circuit voltage [J]. *Energy Environ. Sci*. 2019, **12**(4): 1309-1316.
[27] Yang J, Xiong S, Song J, *et al*. Energetics and energy loss in 2D Ruddlesden-Popper perovskite solar cells [J]. *Adv. Energy Mater*. 2020, **10**(23): 2000687.
[28] Li H, Wu G, Li W, *et al*. Additive engineering to grow micron-sized grains for stable high efficiency perovskite solar cells [J]. *Adv. Sci*. 2019, **6**(18): 1901241.
[29] Arivunithi V M, Reddy S S, Sree V G, *et al*. Efficiency exceeding 20% in perovskite solar cells with side-chain liquid crystalline polymer-doped perovskite absorbers [J]. *Adv. Energy Mater*. 2018, **8**(30): 1801637.
[30] Zheng X, Hou Y, Bao C, *et al*. Managing grains and interfaces via ligand anchoring enables 22.3%-efficiency inverted perovskite solar cells [J]. *Nat. Energy* 2020, **5**(2): 131-140.
[31] Rajagopal A, Yao K, Jen A K Y. Toward perovskite solar cell commercialization: a perspective and research roadmap based on interfacial engineering [J]. *Adv. Mater*. 2018, **30**(32): 1800455.
[32] Bai Y, Meng X, Yang S. Interface engineering for highly efficient and stable planar p-i-n perovskite solar cells [J]. *Adv. Energy Mater*. 2018, **8**(5): 1701883.
[33] Jeong M J, Yeom K M, Kim S J, *et al*. Spontaneous interface engineering for dopant-free poly (3-hexylthiophene) perovskite solar cells with efficiency over 24% [J]. *Energy Environ. Sci*. 2021, **14**(4): 2419-2428.
[34] Liu Z, Siekmann J, Klingebiel B, *et al*. Interface optimization via fullerene blends enables open-circuit voltages of 1.35 V in $CH_3NH_3Pb(I_{0.8}Br_{0.2})_3$ solar cells [J]. *Adv. Energy Mater*. 2021, **11**: 2003386.
[35] Son D Y, Kim S G, Seo J Y, *et al*. Universal approach toward hysteresis-free perovskite solar cell via defect engineering [J]. J. *Am. Chem. Soc*. 2018, **140**(4): 1358-1364.
[36] Abdi Jalebi M, Andaji Garmaroudi Z, Cacovich S, *et al*. Maximizing and stabilizing luminescence from halide perovskites with potassium passivation [J]. *Nature* 2018, **555**(7697): 497-501.
[37] Han T H, Lee J W, Choi C, *et al*. Perovskite-polymer composite cross-linker approach for highly-stable and efficient perovskite solar cells [J]. *Nat. Commun*. 2019, **10**(1): 520.
[38] Zuo L, Guo H, Jariwala S, *et al*. Polymer-modified halide perovskite films for efficient and stable planar heterojunction solar cells [J]. *Sci. Adv*. 2017, **3**(8): e1700106.
[39] Bai S, Da P, Li C, *et al*. Planar perovskite solar cells with long-term stability using ionic liquid additives [J]. *Nature* 2019, **571**(7764): 245-250.
[40] Zhang F, Bi D, Pellet N, *et al*. Suppressing defects through the synergistic effect of a Lewis base and a Lewis acid for highly efficient and stable perovskite solar cells [J]. *Energy Environ. Sci*. 2018, **11**(12): 3480-3490.
[41] Irimia Vladu M. "Green" electronics: biodegradable and biocompatible materials and devices for sustainable future [J]. *Chem. Soc. Rev*. 2014, **43**(2): 588-610.
[42] Zhu H, Luo W, Ciesielski P N, *et al*. Wood-derived materials for green electronics, biological devices, and energy applications [J]. *Chem. Rev*. 2016, **116**(16): 9305-9374.
[43] Lee C J, Chang Y C, Wang L W, *et al*. Biodegradable materials for organic field-effect transistors on a paper substrate [J]. *IEEE Electron Device Lett*. 2019, **40**(2): 236-239.
[44] Li W, Liu Q, Zhang Y, *et al*. Biodegradable materials and green processing for green electronics [J]. *Adv. Mater*. 2020, **32**(33): 2001591.
[45] Jin C, Nai J, Sheng O, *et al*. Biomass-based materials for green lithium secondary batteries [J]. *Energy Environ. Sci*. 2021, **14**(3): 1326-1379.
[46] Zeng M, Wang X, Ma R, *et al*. Dopamine semiquinone radical doped PEDOT: PSS: enhanced conductivity, work function and performance in organic solar cells [J]. *Adv. Energy Mater*. 2020, **10**(25): 2000743.
[47] Li J, Wang N, Wang Y, *et al*. Efficient inverted organic solar cells with a thin natural biomaterial L-Arginine as electron transport layer [J]. *Sol. Energy 2020*, 196: 168-176.
[48] Wang R, Xue J, Wang K L, *et al*. Constructive molecular configurations for surface-defect passivation of perovskite photovoltaics [J]. *Science* 2019, **366**(6472): 1509-1513.
[49] Yang J, Xiong S, Qu T, *et al*. Extremely low-cost and green cellulose passivating perovskites for stable and high-performance solar cells [J]. *ACS Appl. Mater. Interfaces* 2019, **11**(14): 13491-13498.
[50] Lin H S, Lee J M, Han J, *et al*. Denatured M13 bacteriophage-templated perovskite solar cells exhibiting high efficiency [J]. *Adv. Sci*. 2020, **7**(20): 2000782.
[51] Xiong S, Hao T, Sun Y, *et al*. Defect passivation by nontoxic biomaterial yields 21% efficiency perovskite solar cells [J]. J. *Energy Chem*. 2021, **55**: 265-271.
[52] Hou Y, Wang K, Yang D, *et al*. Enhanced performance and stability in DNA-perovskite heterostructure-based solar cells [J]. *ACS Energy Lett*. 2019, **4**(11): 2646-2655.
[53] Das S, Wu C, Song Z, *et al*. Bacteriorhodopsin enhances efficiency of perovskite solar cells [J]. *ACS Appl. Mater. Interfaces* 2019, **11**(34): 30728-30734.
[54] Xie L, Cao Z, Wang J, *et al*. Improving energy level alignment by adenine for efficient and stable perovskite solar cells [J]. *Nano Energy 2020*, 74: 104846.
[55] Zhu K, Lu Z, Cong S, *et al*. Ultraflexible and lightweight bamboo-derived transparent electrodes for perovskite solar cells [J]. *Small* 2019, **15**(33): 1902878.
[56] Salim T, Sun S, Abe Y, *et al*. Perovskite-based solar cells: impact of morphology and device architecture on device performance [J]. J. *Mater. Chem*. A 2015, **3**(17): 8943-8969.
[57] Li G, Ching K L, Ho J Y L, *et al*. Identifying the optimum morpholo-

gy in high-performance perovskite solar cells [J]. *Adv. Energy Mater.* 2015, **5**(9): 1401775.
[58] Wang R, Xue J, Meng L, *et al*. Caffeine improves the performance and thermal stability of perovskite solar cells [J]. *Joule* 2019, **3**(6): 1464-1477.
[59] Chen B, Rudd P N, Yang S, *et al*. Imperfections and their passivation in halide perovskite solar cells [J]. *Chem. Soc. Rev.* 2019, **48**(14): 3842-3867.
[60] Ono L K, Liu S, Qi Y. Reducing detrimental defects for high-performance metal halide perovskite solar cells [J]. *Angew. Chem.*, Int. Ed. 2020, **59**(17): 6676-6698.
[61] Azpiroz J M, Mosconi E, Bisquert J, *et al*. Defect migration in methylammonium lead iodide and its role in perovskite solar cell operation [J]. *Energy Environ. Sci.* 2015, **8**(7): 2118-2127.
[62] Eames C, Frost J M, Barnes P R, *et al*. Ionic transport in hybrid lead iodide perovskite solar cells [J]. *Nat. Commun.* 2015, **6**: 7497.
[63] Zhang S, Shaw P E, Zhang G, *et al*. Defect/interface recombination limited quasi-fermi level splitting and open-circuit voltage in mono- and triple-cation perovskite solar cells [J]. *ACS Appl. Mater. Interfaces* 2020, **12**(33): 37647-37656.
[64] Wang Q, Chen B, Liu Y, *et al*. Scaling behavior of moisture-induced grain degradation in polycrystalline hybrid perovskite thin films [J]. *Energy Environ. Sci.* 2017, **10**(2): 516-522.
[65] Tan S, Ilhan Yavuz M H, Lee J W, *et al*. Shallow iodine defects accelerate the degradation of α-phase formamidinium perovskite [J]. *Joule* 2020, **4**(11): 2426-2442.
[66] Qiu S, Xu X, Zeng L, *et al*. Biopolymer passivation for high-performance perovskite solar cells by blade coating [J]. J. *Energy Chem.* 2021, **54**: 45-52.
[67] Hu J, Xu X, Chen Y, *et al*. Overcoming photovoltage deficit via natural amino acid passivation for efficient perovskite solar cells and modules [J]. J. *Mater. Chem.* A 2021, **9**(9): 5857-5865.
[68] Cahen D, Kahn A. Electron energetics at surfaces and interfaces: concepts and experiments [J]. *Adv. Mater.* 2003, **15**(4): 271-277.
[69] Yang J M, Luo Y, Bao Q, *et al*. Recent advances in energetics and stability of metal halide perovskites for optoelectronic applications [J]. *Adv. Mater. Interfaces* 2019, **6**(3): 1801351.
[70] Lin Y, Chen B, Zhao F, *et al*. Matching charge extraction contact for wide-bandgap perovskite solar cells [J]. *Adv. Mater.* 2017, **29**(26): 1700607.
[71] Schulz P, Edri E, Kirmayer S, *et al*. Interface energetics in organo-metal halide perovskite-based photovoltaic cells [J]. *Energy Environ. Sci.* 2014, **7**(4): 1377-1381.
[72] Wang Q, Shao Y, Xie H, *et al*. Qualifying composition dependent p and n self-doping in $CH_3NH_3PbI_3$ [J]. *Appl. Phys. Lett.* 2014, **105**(16): 163508.
[73] Cui P, Wei D, Ji J, *et al*. Highly efficient electron-selective layer free perovskite solar cells by constructing effective p-n heterojunction [J]. *Sol. RRL* 2017, **1**(2): 1600027.
[74] Olthof S, Meerholz K. Substrate-dependent electronic structure and film formation of $MAPbI_3$ perovskites [J]. *Sci. Rep.* 2017, **7**(1): 40267.
[75] Zohar A, Kulbak M, Levine I, *et al*. What limits the open-circuit voltage of bromide perovskite-based solar cells? [J]. *ACS Energy Lett.* 2019, **4**(1): 1-7.
[76] Zhang J, Yu H. Multifunctional dopamine-assisted preparation of efficient and stable perovskite solar cells [J]. J. *Energy Chem.* 2021, **54**: 291-300.
[77] Xiong S, Hou Z, Zou S, *et al*. Direct observation on p- to n-type transformation of perovskite surface region during defect passivation driving high photovoltaic efficiency [J]. *Joule* 2021, **5**(2): 467-480.
[78] Chen H C, Hung C M, Kuo C H. Synergistic engineering of natural carnitine molecules allowing for efficient and stable inverted perovskite solar cells [J]. *ACS Appl. Mater. Interfaces* 2021, **13**(7): 8595-8605.
[79] Xiong S, Song J, Yang J, *et al*. Defect-passivation using organic dyes for enhanced efficiency and stability of perovskite solar cells [J]. *Sol. RRL* 2020, **4**(5): 1900529.
[80] Dong Q, Zhu C, Chen M, *et al*. Interpenetrating interfaces for efficient perovskite solar cells with high operational stability and mechanical robustness [J]. *Nat. Commun.* 2021, **12**(1): 973.
[81] Chen W, Han B, Hu Q, *et al*. Interfacial stabilization for inverted perovskite solar cells with long-term stability [J]. *Sci. Bull.* 2021, **66**(10): 991-1002.
[82] Ning J, Zhu Y, Hu Z, *et al*. Gaining insight into the effect of organic interface layer on suppressing ion migration induced interfacial degradation in perovskite solar cells [J]. *Adv. Funct. Mater.* 2020, **30**(35): 2000837.
[83] Hu L, Zhao Q, Huang S, *et al*. Flexible and efficient perovskite quantum dot solar cells via hybrid interfacial architecture [J]. *Nat. Commun.* 2021, **12**(1): 466.
[84] Xiong S, Yuan M, Yang J, *et al*. Engineering of the back contact between PCBM and metal electrode for planar perovskite solar cells with enhanced efficiency and stability [J]. *Adv. Opt. Mater.* 2019, **7**(19): 1900542.
[85] Wang B, Yang J, Lu L, *et al*. Interface engineering of air-stable n-doping fullerene-modified TiO_2 electron transport layer for highly efficient and stable perovskite solar cells [J]. *Adv. Mater. Interfaces* 2020, **7**(6): 1901964.
[86] Xiong S, Dai Y, Yang J, *et al*. Surface charge-transfer doping for highly efficient perovskite solar cells [J]. *Nano Energy 2021*, 79: 105505.
[87] Lian J, Lu B, Niu F, *et al*. Electron-transport materials in perovskite solar cells [J]. *Small Methods* 2018, **2**(10): 1800082.
[88] Yang W S, Noh J H, Jeon N J, *et al*. High-performance photovoltaic perovskite layers fabricated through intramolecular exchange [J]. *Science* 2015, **348**(6240): 1234.
[89] Jeong J, Kim M, Seo J, *et al*. Pseudo-halide anion engineering for α-$FAPbI_3$ perovskite solar cells [J]. *Nature* 2021, **592**: 381 - 385.
[90] Leijtens T, Eperon G E, Pathak S, *et al*. Overcoming ultraviolet light instability of sensitized TiO_2 with meso-superstructured organo-metal tri-halide perovskite solar cells [J]. *Nat. Commun.* 2013, **4**(1): 2885.
[91] You S, Wang H, Bi S, *et al*. A biopolymer heparin sodium interlayer anchoring TiO_2 and $MAPbI_3$ enhances trap passivation and device stability in perovskite solar cells [J]. *Adv. Mater.* 2018, **30**(22): 1706924.
[92] Peng X, Lu H, Zhuang J, *et al*. Enhanced performance of perovskite solar cells using DNA-doped mesoporous-TiO_2 as electron transporting layer [J]. *Sol. Energy 2020*, 206: 855-863.
[93] Zhang Y, Liu X, Li P, *et al*. Dopamine-crosslinked TiO_2/perovskite layer for efficient and photostable perovskite solar cells under full spectral continuous illumination [J]. *Nano Energy*, 2019, **56**: 733-740.
[94] Wang B, Li N, Yang L, *et al*. Chlorophyll derivative-sensitized TiO_2 electron transport layer for record efficiency of $Cs_2AgBiBr_6$ double perovskite solar cells [J]. J. *Am. Chem. Soc.* 2021, **143**(5): 2207-2211.
[95] Mokhtar M Z, He J, Li M, *et al*. Bioinspired scaffolds that sequester lead ions in physically damaged high efficiency perovskite solar cells [J]. *Chem. Commun.* 2021, **57**(8): 994-997.
[96] Ke W, Fang G, Liu Q, *et al*. Low-temperature solution-processed tin oxide as an alternative electron transporting layer for efficient perovskite solar cells [J]. J. *Am. Chem. Soc.* 2015, **137**(21): 6730-6733.
[97] Jiang Q, Zhang L, Wang H, *et al*. Enhanced electron extraction using SnO_2 for high-efficiency planar-structure $HC(NH_2)_2PbI_3$-based perovskite solar cells [J]. *Nat. Energy* 2016, **2**(1): 1-7.
[98] Rao H S, Chen B X, Li W G, *et al*. Improving the extraction of photogenerated electrons with SnO_2 nanocolloids for efficient planar perovskite solar cells [J]. *Adv. Funct. Mater.* 2015, **25**(46): 7200-7207.
[99] Hou M, Zhang H, Wang Z, *et al*. Enhancing efficiency and stability of perovskite solar cells via a self-assembled dopamine interfacial layer [J]. *ACS Appl. Mater. Interfaces* 2018, **10**(36): 30607-30613.
[100] Kim G W, Choi Y, Choi H, *et al*. Novel cathode interfacial layer using creatine for enhancing the photovoltaic properties of perovskite solar cells [J]. J. *Mater. Chem.* A 2020, **8**(41): 21721-21728.
[101] Said A A, Xie J, Zhang Q. Recent progress in organic electron transport materials in inverted perovskite solar cells [J]. *Small* 2019, **15**(27): 1900854.
[102] Hawash Z, Ono L K, Qi Y. Recent advances in Spiro-MeOTAD hole transport material and its applications in organic-inorganic halide perovskite solar cells [J]. *Adv. Mater. Interfaces* 2018, **5**(1): 1700623.
[103] Kim H S, Lee C R, Im J H, *et al*. Lead iodide perovskite sensitized all-solid-state submicron thin film mesoscopic solar cell with efficiency exceeding 9% [J]. *Sci. Rep.* 2012, **2**: 591.
[104] Li M, Li Y, Sasaki S i, *et al*. Dopant-free zinc chlorophyll aggregates as an efficient biocompatible hole transporter for perovskite solar cells [J]. *ChemSusChem* 2016, **9**(19): 2862-2869.
[105] Yusoff A R b M, Kim J, Jang J, *et al*. New horizons for perovskite

solar cells employing DNA-CTMA as the hole-transporting material [J]. *ChemSusChem* 2016, **9**(13): 1736-1742.
[106] Yu Z, Sun L. Inorganic hole-transporting materials for perovskite solar cells [J]. *Small Methods* 2018, **2**(2): 1700280.
[107] Reza K M, Mabrouk S, Qiao Q. A review on tailoring PEDOT: PSS layer for improved performance of perovskite solar cells [J]. *Proc. Nat. Res. Soc* 2018, **2**(1): 02004.
[108] Wang Q, Chueh C C, Eslamian M, *et al*. Modulation of PEDOT: PSS pH for efficient inverted perovskite solar cells with reduced potential loss and enhanced stability [J]. *ACS Appl. Mater. Interfaces* 2016, **8**(46): 32068-32076.
[109] Huang J, Wang K X, Chang J J, *et al*. Improving the efficiency and stability of inverted perovskite solar cells with dopamine-copolymerized PEDOT: PSS as a hole extraction layer [J]. J. *Mater. Chem.* A 2017, **5**(26): 13817-13822.
[110] Xue Q, Liu M, Li Z, *et al*. Efficient and stable perovskite solar cells via dual functionalization of dopamine semiquinone radical with improved trap passivation capabilities [J]. *Adv. Funct. Mater*. 2018, **28**(18): 1707444.
[111] Yang D, Yang R, Priya S, *et al*. Recent advances in flexible perovskite solar cells: fabrication and applications [J]. *Angew. Chem.*, Int. Ed. 2019, **58**(14): 4466-4483.
[112] Heo J H, Lee D S, Shin D H, *et al*. Recent advancements in and perspectives on flexible hybrid perovskite solar cells [J]. J. *Mater. Chem.* A 2019, **7**(3): 888-900.
[113] Gao C, Yuan S, Cui K, *et al*. Flexible and biocompatibility power source for electronics: a cellulose paper based hole-transport-materials-free perovskite solar cell [J]. *Sol. RRL* 2018, **2**(11): 1800175.
[114] Han J, Nam J S, Kim K, *et al*. M13 bacteriophage-templated gold nanowires as stretchable electrodes in perovskite solar cells [J]. *Adv. Mater*. 2021, **2**(1): 488-496.